The Fatigue Behavior and Mechanism of Large FV520B-I Specimens in a Very High Cycle Regime

Han Zhang
Qilu University of Technology (Shandong Academy of Sciences)
Ming Zhang (zm870623@foxmail.com)
Qilu University of Technology (Shandong Academy of Sciences)
Li Meng Li
Qilu University of Technology
Bao Hai Xie
Qilu University of Technology
Jun Li Zhang
Ningbo Geely Royal Engine Components Co Ltd

Original Article

Keywords: FV520B-I, Specimen size, Very high cycle fatigue, Statistics of extreme values, Fatigue strength and fatigue life

Posted Date: January 4th, 2021

DOI: https://doi.org/10.21203/rs.3.rs-136150/v1

Title page

The Fatigue Behavior and Mechanism of large FV520B-I specimens in a Very High Cycle Regime

Han, Zhang, born in 1998. He received his bachelor degree from *Qilu University of Technology* (Shandong Academy of Sciences). His major research interests are ultrahigh cycle fatigue and mechanical engineering.
E-mail: 260828436@qq.com

Ming, Zhang, born in 1987, is an associate professor of *Qilu University of Technology* (Shandong Academy of Sciences). He received his doctor degree from *Shandong University*. His main research direction is very high cycle fatigue.
Tel: 13853157623 E-mail: zm870623@foxmail.com

Meng-Li, Li, born in 1987. She received her doctor degree from *Shandong University*.
E-mail: miling001@163.com

Hai-Bao, Xie, born in 1997, He graduated from *Qilu University of Technology* (Shandong Academy of Sciences).
E-mail: 1351164877@qq.com

Li-Jun, Zhang, born in 1984, He received his bachelor degree from *Shandong University.* He worked in *Ningbo Geely Royal Engine Components Co.,Ltd*
E-mail: zhanglj@geely.com

Corresponding author: Ming, Zhang E-mail: zm870623@foxmail.com

ORIGINAL ARTICLE

The Fatigue Behavior and Mechanism of large FV520B-I specimens in a Very High Cycle Regime

Han Zhang[1]• Ming Zhang[1] • Meng-Li Li[1] • Hai-Bao Xie[1] • Li-Jun Zhang[2]

ABSTRACT: We examined the fatigue properties in very high cycle regime of large FV520B-I specimens in an ultrasonic fatigue test. The fatigue mechanism in very high cycle regime didn't change and the fatigue properties obviously degraded as the specimen size enlarged. The fatigue life decreased and the S-N curve moved downward due to the increase of inclusion size in large specimens. The maximum inclusion sizes in specimens were predicted by the method of statistics of extreme value. The prediction of fatigue strength using the modified Murakami model was closer to the test result, and the fitting of fatigue life using the corrosion fatigue crack initiation life model was less effective compared with the fitting of small specimen test results

Keywords: FV520B-I·Specimen size·Very high cycle fatigue·Statistics of extreme values·Fatigue strength and fatigue life

✉Ming Zhang E-mail: zm870623@foxmail.com

1 Qilu University of Technology (Shandong Academy of Sciences), Jinan 3501 Daxue Road, China

2 NO.818, Binhai No.2 Road, Hangzhou Bay New District, Ningbo, China

1 Introduction

Several failure cases show that fatigue is the main failure mode of centrifugal compressor impellers [1, 2]. With the economy development and the constraint enhancement of the environment and resources, there is a higher demand for the impeller life. The impeller fatigue life should be exceed 10^7 cycles and into the very high cycle fatigue (VHCF) regime. Current research on impeller VHCF is rare. FV520B-I is an important material of centrifugal compressor impellers and is belong to martensitic precipitated hardening stainless steel. We had studied the VHCF of small FV520B-I specimens, which revealed that the cracks in the VHCF regime usually initiate from subsurface inclusions [3-5]. The maximum inclusion size (MIS) in the control volume of specimens is different to determine as the specimen size varies, and the VHCF properties of specimens with different sizes also seem different [6-8]. So it is important to study the effects of specimen size on the VHCF properties. The VHCF properties of a large FV520B-I specimen were tested and compared with previous experiment results of a small FV520B-I specimen.

2 Material and test method

2.1. Material

The chemical components and mechanical properties of FV520-I are showed in Table 1 and Table 2.

Table 1 Chemical composition wt%

C	Si	Mn	P	S	Ni
≤0.07	≤0.07	≤1.0	≤0.03	≤0.03	5.0-6.0
Cr	Cu	Nb	Mo	Fe	
13.2-14.5	1.3-1.8	0.25-0.45	1.3-1.8	Bal.	

Table 2 Mechanical properties

E/GPa	R_m/MPa	$R_{p0.2}$/MPa	*HV*/kgf·mm^2	*A*/%
194	1170	1029	380	16.07

Note: E: Elasticity modulus R_m: Tensile strength

$R_{p0.2}$: Yield strength *HV*: Vickers hardness

A: Elongation

2.2. Test method

Relevant fatigue tests were conducted on a Shimadzu USF-2000. The resonance frequency is 20 kHz, and the stress ratio *R* is -1. We also adopted a specimen with funnel shape that we had previously used for the ultrasonic fatigue tests, and the minimum cross-section diameter of specimen enlarged from 3mm to 5mm. The specimen dimension determined by analytic calculation as shown in Figure1 (b) [5, 9], while the dimension of a small specimen which we previously tested is shown in Fig. 1 (a). The work time and interval were set as 200ms and 600ms. The tests were conducted in air ambient and at room temperature, and the specimen during testing was cooled by the compressed cold air. The specimens were sequential polished with 600, 1000, 2000 mesh emery papers.

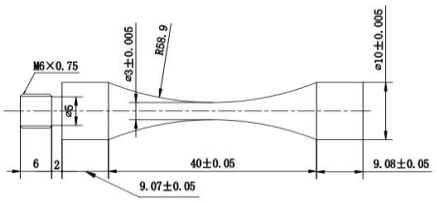

(a) Small specimen

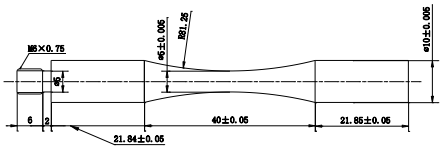

(b) Large specimen

Figure 1 Specimen dimensions (in mm).

3 Experimental results

3.1. Microstructure

The ferrites were distributed in the tempered sorbites, and the granular carbides were observed distributed within the matrix as shown in Figure 2

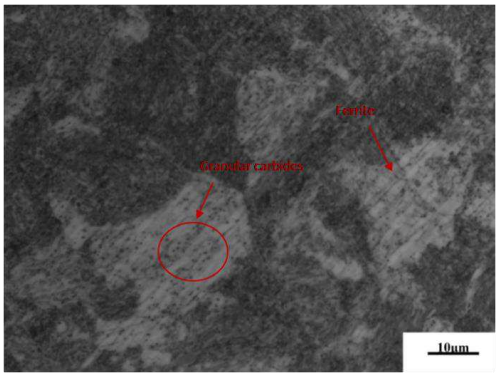

Figure 2 FV520B-I microstructure observation

3.2. VHCF *S-N* Curve

The VHCF *S-N* curves of different size specimens are shown in Figure 3 The small specimens generally fractured in the subsurface, and one specimen fractured on the surface [4], while all large specimens fractured in the subsurface. Compared with the test results of small specimens, the *S-N* curve of large specimens moved downward and the fatigue life of large specimens decreased. The difference of fatigue life between the two types of specimens had an increasing trend as the stress declined, and the maximum difference was up to 10 times. The maximum stress level without fracturing for small specimens was 550MPa, and for large specimen it was 525MPa.

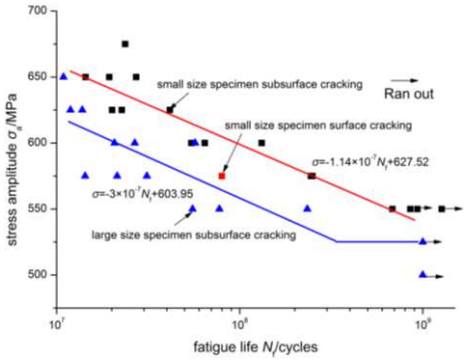

Figure 3 The VHCF *S-N* curves

3.3. The Observation of Fracture Surface

The fractures were observed by a Scanning Electron Microscope. All cracks initiated from subsurface inclusions, and the cracks mostly initiated from single inclusions while some cracks initiated from clusters as shown in Figure 4 All inclusions were identified as Al_2O_3 by energy spectrum analysis, as shown in Figure 5.

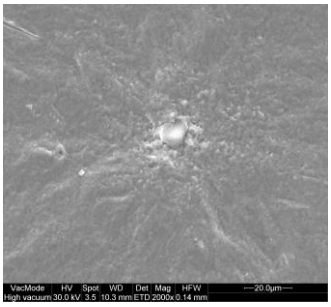

(a) Initiation from a single inclusion (σ_a=575MPa, N_f=1.43×10^7)

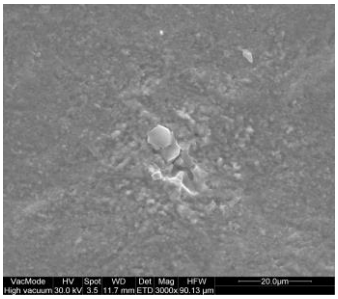

(b) Initiation from a cluster (σ_a=575MPa, N_f=2.14×10^7)

Figure 4 Initiation modes of FV520B-I VHCF cracks in large specimens

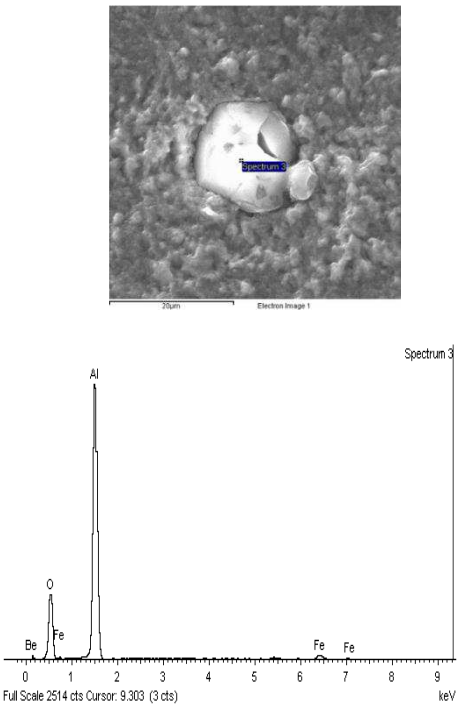

Figure 5 The energy spectrum analysis of an inclusion (σ_a=550MPa, N_f=5.53×10^7)

The cracks propagated and formed a granular bright facet (GBF) after the cracks initiated from inclusions, as shown in Figure 6 The GBF seemed relatively rough and different from the smooth and flat region of the usual crack origin. Also, there was a relatively flat region close to the specimen surface which looked like a fish eye, as shown in Figure 7.

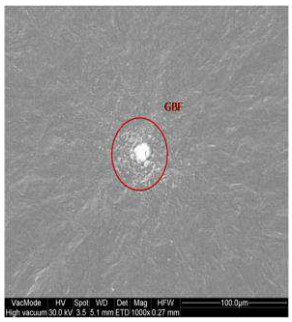

Figure 6 The GBF observation (σ_a=550MPa, N_f=5.53×10^7)

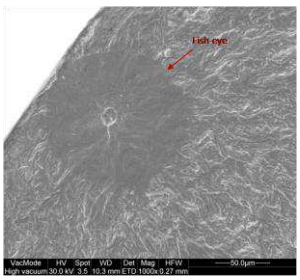

Figure 7 The fish-eye observation (σ_a=625MPa, N_f=1.19×10^7)

3.4 Characteristic Area Size

The distance from the crack origin to the specimen surface, the fish-eye diameter, the GBF diameter, and the inclusion diameter were measured and listed in Table 3.

Table 3 Characteristic area sizes of the fractures

σ_a/MPa	$N_f/10^7$ cycles	d/μm	d_F/μm	$d_{G/}$μm	d_I/μm
650	1.09	307	539	71.5	14.8
625	1.19	67	133	50.0	14.4
625	1.38	887	1529	49.2	11.8
600	2.07	462	685	83.2	16.3
600	2.67	110	203	68.4	11.4
600	5.71	230	407	107.1	13.8
575	1.43	1267	2133	84.1	11.9
575	2.14	1012	1867	90.5	8.6(cluster)
575	3.11	1055	1839	82.4	8.2(cluster)
550	5.53	794	1250	126.9	16.4(cluster)
550	7.75	173	258	130.0	10.9
550	23.4	239	417	99.8	13.2

Note: σ_a: Stress amplitude N_f: Fatigue life d: Distance from the crack origin to the specimen surface d_F: Fish-eye diameter d_G: GBF diameter d_I: Inclusion diameter

3.5 The Statistics of Inclusion Sizes in FV520B-I

The sight area S_0=0.0195mm^2 observed by an optical microscope with a magnification of 200 times was defined as the standard inspection area. FV520B-I VHCF cracks usually initiated from spherical Al_2O_3, so the sizes of MnS inclusions with the shape of a thin strip were not involved. The square root of the maximum inclusion area in S_0 is about the maximum inclusion diameter. There were six specimens, and the observation was repeated 10 times for each specimen. Every observation was selected at random and they did not overlap. The statistical results of the maximum inclusion diameters are shown in Table 4, and the photo of the 40th observation is shown in Figure 8.

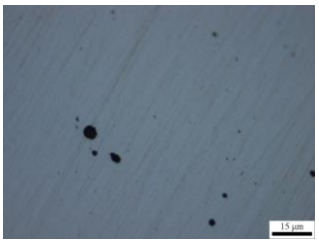

Figure 8 The inclusion situation of the 40th observation

Table 4 The statistical results of the maximum inclusion diameters in the standard inspection areas

No.	D_{max}/μm	No.	D_{max}/μm	No.	D_{max}/μm
1	2.71	21	5.47	41	3.20
2	5.25	22	1.55	42	3.87
3	4.05	23	5.60	43	3.26
4	2.82	24	7.23	44	3.48
5	2.09	25	8.79	45	4.08
6	2.94	26	2.58	46	1.56
7	3.56	27	6.45	47	5.34
8	2.78	28	5.36	48	3.17
9	2.93	29	7.18	49	1.38
10	3.78	30	6.70	50	2.40
11	2.76	31	4.50	51	3.46
12	2.56	32	7.20	52	2.67
13	2.30	33	2.92	53	2.10
14	2.02	34	6.99	54	2.77
15	2.63	35	2.58	55	2.41
16	3.96	36	10.35	56	3.27
17	2.25	37	7.21	57	2.48
18	2.72	38	6.33	58	3.14
19	2.75	39	9.87	59	3.10
20	1.80	40	7.42	60	2.59

Note：No. 1-10, 11-20, 21-30, 31-40, 41-50, and 51-60 are the statistical results for specimen 1, 2, 3, 4, 5, and 6, respectively

4 Discussion

4.1 The Statistics of Extreme Values of the Maximum Inclusion Sizes in VHCF Specimens

A subsurface inclusion is the usual VHCF crack origin [10-14], which has significant effects on the VHCF properties. Due to the low number of large inclusions and the limitation of traditional detection methods, the detection of large inclusions in steel is difficult. At present, the MIS in a large volume is estimated by the extrapolation of inclusion data in a small volume, and the fatigue properties and reliability of steel structure are further predicted by the maximum

inclusion size [15, 16]. The statistics of extreme values (SEV) is an important method to estimate the MIS in a large volume, which is more suitable for steel with large inclusions [9].

SEV [9] predicts the MIS in a large range of steel based on the measured inclusion size in a small randomly selected area or volume [13, 17]. The basic idea of SEV is that the maximum values of each group of data are subject to the same distribution as all data points subject to a distribution. This distribution is usually the Gumbel distribution. The distribution function is as follows:

$$G(z_v)=\exp\left(-\exp\left(-(z_v-\mu)/\theta\right)\right) \tag{1}$$

Where $G(z_v)$ is the probability that the MIS is less than or equal to z_v, and θ, and μ are scale parameter and position parameter, respectively.

The characteristic MIS z_v in different volumes V can be estimated according to Eq. (2):

$$z_v=\theta\left(-\ln\left(-\ln\left((T-1)/T\right)\right)\right)+\mu \tag{2}$$

Where T is the return period:

$$T=V/V_0 \tag{3}$$

Where V_0 is the standard inspection volume:

$$V_0=h\times S_0 \tag{4}$$

Where S_0 is the standard inspection area and h is the average diameter of inclusions

$$h=\frac{\sum_{i=1}^{N}\sqrt{A_{\max,i}}}{N} \tag{5}$$

$\sqrt{A_{\max,i}}$ is about the maximum inclusion diameter in the standard inspection area obtained by the ith observation, in units of μm.

The control volume V has great effects on the maximum inclusion size z_v predicted by the SEV method, so the determination of the control volume of VHCF specimen is important. VHCF specimens are funnel-shaped in this paper. A schematic diagram of its shape and size are shown in Figure 9.

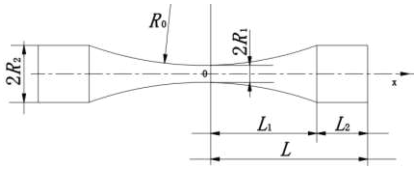

Figure 9 The shape of a funnel specimen

Strain $\varepsilon(x)$ and stress $\sigma(x)$ in the specimen cross-section which is along the x axis is shown in Eq. (6):

$$\left.\begin{aligned}\varepsilon(x)&=\frac{\mathrm{d}U(x)}{\mathrm{d}x}\\ \sigma(x)&=E\varepsilon(x)\end{aligned}\right\} \tag{6}$$

The displacement of specimen in the x-axis direction $U(x)$ is shown in Eq. (7):

$$\left.\begin{aligned}U(x)&=A_0\cos\left[k(L-x)\right],L_1<|x|\le L\\ U(x)&=A_0\varphi\frac{\sinh(\beta x)}{\cosh(\alpha x)},|x|\le L_1\end{aligned}\right\} \tag{7}$$

Where A_0 is the displacement of the specimen end. Variables in Eq. (7) are calculated according to Eqs. (8)-(10):

$$\left.\begin{aligned}\beta&=\sqrt{\alpha^2-k^2}\\ \varphi&=\frac{\cos(kL_2)\cosh(\alpha L_1)}{\sinh(\beta L_1)}\end{aligned}\right\} \tag{8}$$

$$\alpha=\frac{1}{L_1}\arccos h\left(\frac{R_2}{R_1}\right) \tag{9}$$

$$k=\omega/c,\omega=2\pi f,c=\sqrt{\frac{E}{\rho}} \tag{10}$$

Where E is the elasticity modulus, ρ is the material density, and f is the resonance frequency. For funnel shaped specimens, the maximum stress σ_{max} appears in the minimum cross-section of the specimen where x=0, and the test specimen is usually broken at this position. The stress is decreased as the position shifts to each side. The control volume is supposed to be the volume where the stress is higher than $0.9\sigma_{max}$. When the stress is equal to $0.9\sigma_{max}$, x-axis coordinates are $-l_x$ and l_x, respectively. Then the control volume $V=2\pi l_x R_1^2$ [16].

For FV520B-I, when E=194GPa, ρ=7820kg·m^{-3}, and f=20kHz, the sizes of two types of specimens are shown in Fig. 1. According to Eqs. (6)-(10), when R_1=1.5mm, l_x=3.43mm, and V=48.47mm^3. According to Eqs. (3)-(5) and Table 4, $T=V/V_0\approx6.2\times10^5$. Similarly, as the specimen size increases to R_1=2.5mm, l_x=4.79mm, V=188.1mm^3, and T=2.4×10^6.

The Gumbel distribution is usually used in the SEV analysis. The maximum inclusion diameters in Table 4 were fitted by Gumbel distribution using the gum.fit function in ISMEV package of R software which is a statistical analysis software, and we found that when μ=3.100 and θ=1.410,

and T=6.2×10^5, T=2.4×10^6, θ=1.410, and μ=3.100 are substituted into Eq. (2), the maximum inclusion diameters in VHCF specimens can be estimated as z_{v1}=21.91μm and z_{v2}=23.82μm when R_1 is equal to 1.5mm and 2.5mm. The possible maximum inclusion diameter in VHCF specimens increases with an increase of the control volume. z_{v1} is larger than the maximum single inclusion diameter 15.6μm and cluster inclusion diameter 16.4μm on the fatigue fractures of small specimens[5]. z_{v2} is larger than the maximum single inclusion diameter 16.3μm and cluster inclusion diameter 16.4μm on the fatigue fractures of large specimens, as shown in Table 3.

4.2 Effects of Specimen Size on FV520B-I VHCF

The VHCF cracks of small specimens mostly initiated from the subsurface inclusions and only one crack initiated from the surface, while two cracks initiated from the subsurface matrix [5]. All VHCF cracks of large specimens initiated from the interface of the matrix-inclusion, and the inclusions were not cracked, as shown in Figure 4. This phenomenon is in accordance with the test results of small specimen [4, 5] and the usual initiation mode of subsurface cracks in high strength steel [18]. The cracks propagated and formed the GBF after the cracks initiated from the interface of the matrix-inclusion, as shown in Figure 6. There are different views about the GBF formation [19, 20], but most scholars generally think that the hydrogen is an important reason [21, 22]. The effects of hydrogen seem to weaken as the crack grows [23]. The cracks may stably grow only under the mechanical load as the effects of hydrogen disappear. A subsurface crack quickly transforms into a surface crack and the stress intensity factor of the crack suddenly increases. The large difference of crack growth rates in the two parts results in the fish-eye formation, as shown in Figure 7. From section 4.1, the possible maximum inclusion diameter in specimens is increased because the control volume increased with an increase of VHCF specimen size. The actual inclusion sizes at the crack origins of the two groups of specimens were further examined. For large specimens, the maximum inclusion diameter was 16.4μm, the average inclusion diameter was 12.6μm, and the minimum inclusion diameter was 8.2μm as shown in Table 3. For small specimens, the maximum inclusion diameter was 16.4μm, the average inclusion diameter was 12.1μm, and the minimum inclusion diameter was only 4.4μm [5]. The inclusion diameter increased with an increase of specimen size, and which increased the probability of a crack initiating from the inclusion. Therefore, all VHCF cracks in large specimens initiated from the subsurface inclusions, and no crack initiated from surface or subsurface matrix. In addition, an increase of specimen size had no obvious effects on the FV520B-I VHCF mechanism.

The *S-N* curve moved downward as the specimen size increased as shown in Figure 3. The fatigue life of the large specimens was reduced and the reduction seems more obvious in the lower stress, and the fatigue strength up to 10^9 cycles was also decreased. Above phenomenon is caused by two factors. First, the MIS in a specimen increases with an increase of control volume, and the increase of the MIS reduces the fatigue strength of the specimen. Second, the heat effects of large specimens may also affect the fatigue properties.

4.3 The Relationships of Characteristic Area Sizes and VHCF Life

The relationships of characteristic area sizes with VHCF life are shown in Figure 10.

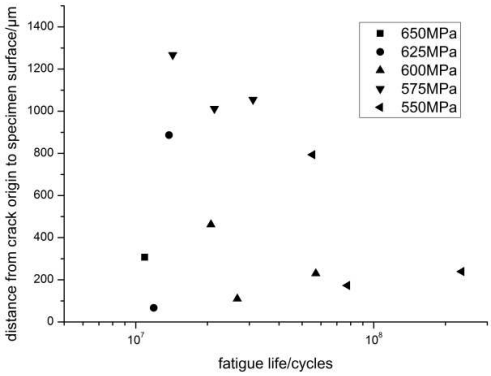

(a) Relationship with the distance from the crack origin to the specimen surface

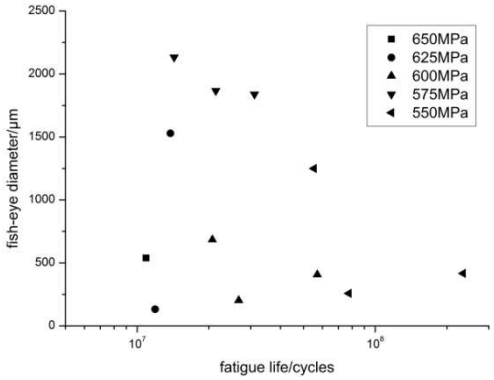

(b) Relationship with the fish-eye diameter

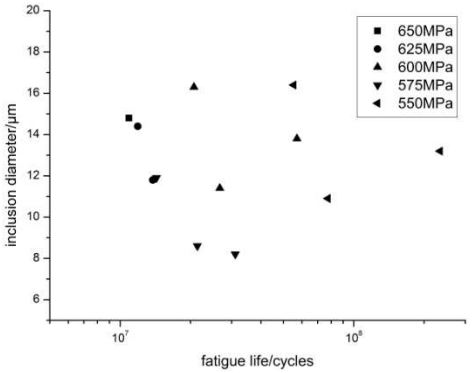

(c) Relationship with the inclusion diameter

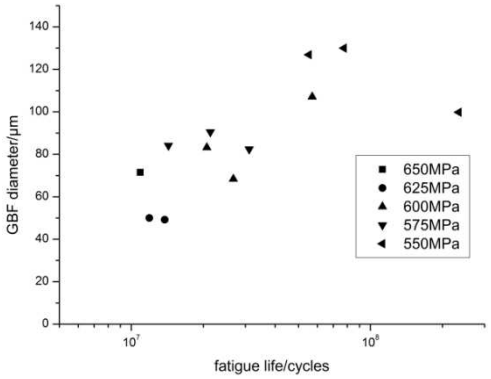

(d) Relationship with the GBF diameter

Figure 10 Relationships of VHCF life of large FV520B-I specimens with the characteristic area sizes

It is similar to the previous small specimen test results that the relationships of the VHCF life of large specimens with regard to the distance from the crack origin to the specimen surface, and with the fish-eye diameter being not obvious as shown in Figure 10 (a), (b). Above results suggest that the crack grows fast outside the GBF and the VHCF life is mainly consumed in the GBF formation. The distribution of data points in both figures are similar, the fish-eye diameter is about two times the distance from the crack origin to the specimen surface, which further testifies that the fish-eye formation is caused by the transition from a subsurface crack to a surface crack.

There is no significant relationship between the VHCF life and the inclusion diameter as illustrated in Figure 10 (c). The subsurface inclusion diameter has a decreasing trend with an increase of fatigue life if the load is constant. When the load is 600MPa or 550MPa, there is a data point at which that its inclusion diameter increases with an increase of fatigue life. Related researches showed that the initiation life of a crack which initiates from the subsurface inclusion appears nearly inversely proportional to the inclusion diameter [18]. So the initiation life may be not the main part of the VHCF life. This conclusion is consistent with the conclusion of small specimen test results [5].

The relationship of VHCF life with the GBF diameter was further investigated as illustrated in Figure 10 (d). The GBF diameter basically increases with an increase of fatigue life. But this trend is not obvious when the load is constant, and sometimes the GBF diameter decreases with an increase of fatigue life, which is very different from the small specimen test results [5].

Small specimen test results showed that the inclusion diameter has a certain effect on the GBF diameter, and the test results of large specimens also showed this. Therefore, we further investigated the relationship of VHCF life of large specimen and the ratio of the GBF diameter to the inclusion diameter, as illustrated in Figure 11. This ratio basically increases with an increase of fatigue life. This increasing trend is more obvious if the load is constant. But with loads of 575MPa and 550MPa, there are data points at which above ratio decrease with an increase of fatigue life. There is an increasing trend of VHCF life when above ratio increases. The crack initiation life increases with a decrease of the inclusion diameter, and the crack propagation life increases with an increase of the GBF diameter.

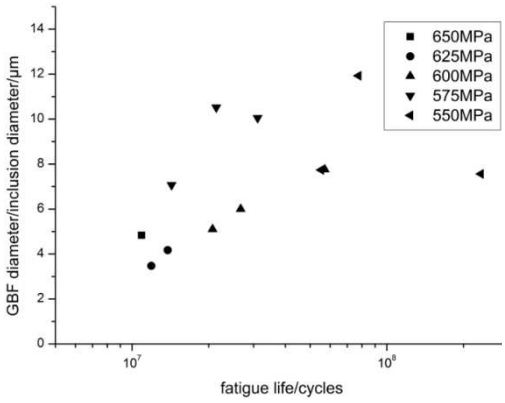

Figure 11 Relationships of VHCF life of large FV520B-I specimens with the ratio of the GBF diameter to the inclusion diameter

4.4 The Predictions of VHCF Strength and VHCF Life

The Murakami model is widely used to predict the VHCF strength. In the case of containing subsurface inclusions, the fatigue strength can be expressed as [10,11]:

$$\sigma_{\mathrm{w}} = \frac{1.42\times(HV+120)}{a^{1/6}} \tag{11}$$

We used the effects of the inclusion shape and modified above model. The modified model is as follows[24]:

$$\sigma_{\mathrm{w}} = \frac{1.45\times(HV+120)}{a^{1/6}} \tag{12}$$

Where HV is the Vickers hardness, in units of kgf·mm^{-2} and a is the inclusion radius, in units of μm. For large specimens, HV of 380 kgf·mm^{-2} and a of 8.2μm are substituted into Eqs. (11) and (12), and σ_{w} equals 500MPa and 510MPa, respectively. The fatigue strength at 10^9 cycles of large specimens was about 525MPa which was obtained by the *S-N* curve in Figure 3, and the prediction value of the modified model was closer to the test result. From section 4.1, the possible maximum inclusion diameters obtained by SEV were 21.91μm and 23.82μm for small specimens and large specimens. The Vickers hardness of 380kgf·mm^{-2} and the possible maximum inclusion radii of 10.96μm and 11.91μm were substituted into Eq. (11), and the low limits of fatigue strength of the two groups of specimens were 477MPa and 470MPa, respectively. The possible maximum inclusion diameter slightly increased and the fatigue strength slightly decreased because the control volume slightly increased. Considering the effects of the inclusion shape, the Vickers hardness of 380kgf·mm^{-2}, and the possible maximum inclusion radii of 10.96μm and 11.91μm were substituted into the Eq. (12), and the low limits of fatigue strength of two groups of specimens were 487MPa and 480MPa, respectively.

The VHCF life is mainly consumed in the GBF formation, and the GBF formation is due to the synergistic actions of hydrogen embrittlement and fatigue. Also, the maximum GBF diameter of small specimens was 121μm [5] and the maximum GBF diameter of large specimens was 130μm as obtained from Table 3, which are smaller than the usual definition size（250-300μm）of a corrosion fatigue initiation crack [25]. So we assumed that the GBF formation is similar to the initiation of the corrosion fatigue crack. As most VHCF cracks initiate from subsurface inclusions, the subsurface inclusion was further regarded as a spherical cavity. Then we tried to predict the VHCF life by the initiation life of the corrosion fatigue crack around the spherical cavity.

Concerning the corrosion fatigue of high strength steel, crack initiation is usually caused by hydrogen embrittlement. Under the action of cyclic stress, the movement of dislocation transports hydrogen atoms to the triaxial stress region in the notch root. Then hydrogen embrittlement occurs and results in corrosion fatigue. Hirose thought that the initiation of the corrosion fatigue crack (CFC) is similar to the initiation of the stress corrosion crack, and derived a CFC initiation life model of a specimen with a notch by the dislocation dipole model [26]:

$$K_{\rho\mathrm{a}}\Big/\sqrt{\pi\rho}-\left(K_{\rho\mathrm{a}}\Big/\sqrt{\pi\rho}\right)_{\mathrm{th}} = B_1 + B_2\ln N_{\mathrm{i}} \tag{13}$$

B_1 and B_2 are the constants related to the hydrogen diffusion coefficient and the loading frequency, $K_{\rho\mathrm{a}}$ is the stress intensity factor amplitude in the notch root, ρ is the curve radius of the notch, N_{i} is the CFC initiation life, and the CFC initiation threshold $\left(2K_{\rho\mathrm{a}}\Big/\sqrt{\pi\rho}\right)_{\mathrm{th}}$ is equal to the yield shear strength of high strength steel [26]. In the situation of a VHCF crack initiating from a subsurface inclusion, we assumed that the inclusion was a spherical cavity and approximately calculated $K_{\rho\mathrm{a}}$ by regarding the spherical cavity as a circular crack of infinite volume [27], then:

$$K_{\rho\mathrm{a}} = 2\sigma_{\mathrm{a}}\sqrt{\frac{a}{\pi}} \tag{14}$$

Where a is the inclusion radius, ρ is equal to the spherical cavity radius and the inclusion radius a:

$$\frac{K_{\rho a}}{\sqrt{\pi\rho}} = \frac{2}{\pi}\sigma_a \tag{15}$$

Assume N_i equals the GBF formation life, and is approximately equal to the VHCF life N_f. The yield shear strength is estimated by 0.7 times yield strength. Then we can obtain the equation:

$$\frac{2}{\pi}\sigma_a - 0.35R_{p0.2} = B_1 + B_2 \ln N_f \tag{16}$$

There is a linear relationship between $\left(\frac{2}{\pi}\sigma_a - 0.35R_{p0.2}\right)$ and $\ln N_f$ according to Eq. (16). The relevant test data of small specimens were linearly fitted via the least squares principle and the result is shown in Figure 12.

We obtained B_1=333.2, B_2=-16.80, and r2=0.871. Compared with the fitting result based on crack propagation in the GBF following the Paris law [5], the CFC initiation life model coincides well with the test data, and indirectly confirms the feasibility of research on the VHCF life by CFC initiation. Also, the CFC initiation life model only reflects the relationship of stress amplitude and fatigue life, so it was determined that the stress amplitude seems to be the main factor influencing the VHCF life.

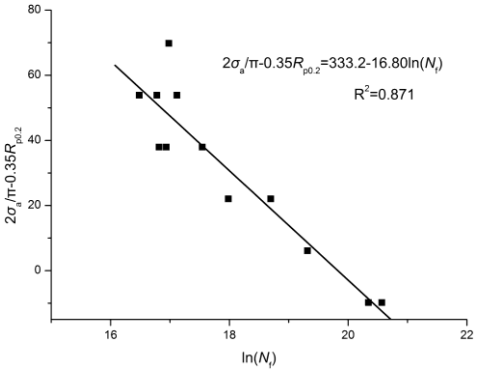

Figure 12 The fitting results of test data of small specimens by the corrosion fatigue crack initiation life model.

The fitting results of the test data of large specimens by the corrosion fatigue crack initiation life model is shown in Figure 13. From Figure 13 and Eq. (16), we obtained B_1=310.35, B_2=-17.13, and r2=0.563. Compared with the fitting for the VHCF life of small specimens by the above model, the fitting deviation of the VHCF life of large specimens seems large. There is an obvious linear relationship of σ_a and lnN_f for small specimens and the weaker linear relationship of σ_a and lnN_f for large specimen result in the above phenomenon, and the weaker linear relationship of σ_a and lnN_f for large specimens is caused even less by the fatigue life under 575MPa than the fatigue life under 600MPa. The heat effects of large specimens were significantly higher than that of small specimens, which may be the main reason for the above abnormal phenomenon.

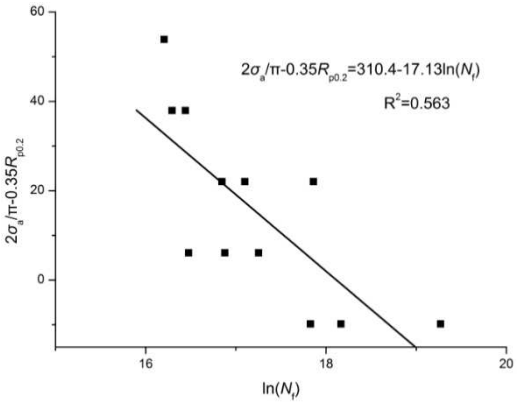

Figure 13 The fitting results of test data of large specimens by the CFC initiation life model

5 Conclusions

It can be concluded that:

(1) For FV520B-I, the VHCF mechanism did not change as specimen size increases. The *S-N* curve moves downward, and fatigue life is reduced and the fatigue strength up to 10^9 cycles decreases for large specimens. The main reason for the above phenomenon is that the control volume increases with an increase of specimen size, and the maximum inclusion size in large specimens is increased.

(2) There are no obvious relationships between the VHCF life with the fish-eye diameter, with the distance from the crack origin to the specimen surface. When the load is constant, the VHCF life basically increases with an increase of the ratio of the GBF diameter to the inclusion diameter and with a decrease of inclusion diameter. The VHCF life is mainly consumed in the GBF formation.

(3) The VHCF strength and VHCF life of large specimens were predicted or fitted through the Murakami model, the modified Murakami model involving effects of inclusion shape, and the CFC initiation life model. Compared with the

prediction of small specimen test results, the prediction of fatigue life was less effective and the prediction of fatigue strength using the modified model was closer to the test result.

6 Declaration

Acknowledgements

Thanks to Dr. Edward C. Mignot, Shandong University, for linguistic advice.

Funding

The authors gratefully acknowledge the financial support provided by National Natural Science Foundation of China (Grant No. 51705265).

Availability of data and materials

The datasets supporting the conclusions of this article are included within the article.

Authors' contributions

The author' contributions are as follows: Zhang Ming and Li Mengli were in charge of the whole trial; Zhang Han wrote the manuscript; Xie Haibao assisted with sampling and laboratory analyses. Zhang Lijun provided technical support.

Competing interests

The authors declare no competing financial interests.

Consent for publication

Not applicable

Ethics approval and consent to participate

Not applicable

REFERENCES

[1] Sivaprasad, S., Narasaiah, N., Das, S. K., Das, G., Tarafder, S., Gupta, K. K., and Ghosh, R. N., 2010, Investigation on the failure of air compressor, *Engineering Failure Analysis,* 17(1), pp. 150-157.

[2] Zhang, M., Liu, Y., Wang, W., Wang, P., and Li, J., The fatigue of impellers and blades, *Engineering Failure Analysis*, 2016,62, pp. 208-231.

[3] Zhang, M., Wang, W., Wang, P., Liu, Y., and Li, J. Fatigue behavior and mechanism of FV520B-I welding seams in a very high cycle regime," *International Journal Of Fatigue*, 2016, 87, pp. 22-37.

[4] Zhang, M., Wang, W. Q., Wang, P. F., Liu, Y., and Li, J. F., , Fatigue Behavior and Mechanism of FV520B-I in Ultrahigh Cycle Regime, *Procedia Materials Science*, 2014,3(0), pp. 2035-2041.

[5] Zhang, M., Wang, W., Wang, P., Liu, Y., and Li, J., Fatigue behavior and mechanism of FV520B in very high cycle regime, *Strength, Fracture and Complexity*, 2015,9(2), pp. 161-174.

[6] Furuya, Y., Size effects in gigacycle fatigue of high-strength steel under ultrasonic fatigue testing, *Procedia Engineering*, 2010, 2(1), pp. 485-490.

[7] Furuya, Y., Notable size effects on very high cycle fatigue properties of high-strength steel, *Materials Science and Engineering: A*, 2011, 528(15), pp. 5234-5240.

[8] Furuya, Y., Specimen size effects on gigacycle fatigue properties of high-strength steel under ultrasonic fatigue testing, *Scripta Mater*, 2008, 58(11), pp. 1014-1017.

[9] Li, S. X., Weng, Y. Q., Hui, W. J., and Yang, Z. G., Very High Cycle Fatigue Properties of High Strength Steels-Effects of Nonmetallic Inclusion, Metallurgical Industry Press, Beijing, 2010.

[10] Chapetti, M. D., Tagawa, T., and Miyata, T., Ultra-long cycle fatigue of high-strength carbon steels part I: review and analysis of the mechanism of failure, Materials Science and Engineering: A, 2003, 356(1–2), pp. 227-235.

[11] Chapetti, M. D., Tagawa, T., and Miyata, T., Ultra-long cycle fatigue of high-strength carbon steels part II: Estimation of fatigue limit for failure from internal inclusions, *Materials Science and Engineering A*, 2003, 356(1-2), pp. 236-244.

[12] Murakami, Y., and Endo, M., Effects of defects, inclusions and inhomogeneities on fatigue strength, *International Journal Of Fatigue*, 1994, 16(3), pp. 163-182.

[13] Murakami, Y., Kodama, S., and Konuma, S., Quantitative evaluation of effects of non-metallic inclusions on fatigue strength of high strength steels. I: Basic fatigue mechanism and evaluation of correlation between the fatigue fracture stress and the size and location of non-metallic inclusions, *International Journal Of Fatigue*, 1989, 11(5), pp. 291-298.

[14] Wang, Q. Y., Bathias, C., Kawagoishi, N., and Chen, Q., Effect of inclusion on subsurface crack initiation and gigacycle fatigue strength, *International Journal Of Fatigue*, 2002, 24(12), pp. 1269-1274.

[15] Sun, C. Q., Lei, Z. Q., Xie, J. J., and Hong, Y. S., Effects of inclusion size and stress ratio on fatigue strength for high-strength steels with fish-eye mode failure, *International Journal Of Fatigue*, 2013, 48(0), pp. 19-27.

[16] Li, W., Sakai, T., Wakita, M., and Mimura, S., Influence of microstructure and surface defect on very high cycle fatigue properties of clean spring steel, *International Journal Of Fatigue*, 2014, 60(0), pp. 48-56.

[17] Murakami, Y., and Usuki, H., Quantitative evaluation of effects of non-metallic inclusions on fatigue strength of high

strength steels. II: Fatigue limit evaluation based on statistics for extreme values of inclusion size, *International Journal Of Fatigue*, 1989, 11(5), pp. 299-307.

[18] Tanaka, K., and Mura, T., A theory of fatigue crack initiation at inclusions, *Metallurgical Transactions A*, 1982, 13(1), pp. 117-123.

[19] Murakami, Y., Nomoto, T., and Ueda, T., Factors influencing the mechanism of superlong fatigue failure in steels, *Fatigue and Fracture of Engineering Materials and Structures*, 1999, 22(7), pp. 581-590.

[20] Shiozawa, K., Morii, Y., Nishino, S., and Lu, L., Subsurface crack initiation and propagation mechanism in high-strength steel in a very high cycle fatigue regime, *International Journal Of Fatigue*, 2006, 28(11), pp. 1521-1532.

[21] Murakami, Y., and Matsunaga, H., The effect of hydrogen on fatigue properties of steels used for fuel cell system, *International Journal Of Fatigue*, 2006, 28(11), pp. 1509-1520.

[22] Otsuka, T., Hanada, H., Nakashima, H., Sakamoto, K., Hayakawa, M., Hashizume, K., and Sugisaki, M., Observation of hydrogen distribution around non-metallic inclusions in steels with tritium microautoradiography, *Fusion Sci Technol*, 2005, 48, pp. 708-711.

[23] Liu, Y. B., Yang, Z. G., Li, Y. D., Chen, S. M., Li, S. X., Hui, W. J., and Weng, Y. Q., On the formation of GBF of high-strength steels in the very high cycle fatigue regime, *Materials Science and Engineering A*, 2008, 497(1-2), pp. 408-415.

[24] Ming, Z., Weiqiang, W., Pengfei, W., Yan, L., and Jianfeng, L., The prediction for fatigue strength in very high cycle regime of high strength steel, *Strength, Fracture and Complexity,*2016.

[25] Wang, R., The corrosion fatigue of metal material, Northwestern Polytechnical University Press, Xi'an, 2001.

[26] Hirose, Y., and Mura, T., Crack nucleation and propagation of corrosion fatigue in high-strength steel, *Engineering Fracture Mechanics*, 1985, 22(5), pp. 859-870.

[27] Acadamy, C. A., The stress analysis of cracks handbook, Science Press, Beijing, 1993.

Biographical notes

Han, Zhang, born in 1998. He received his bachelor degree from *Qilu University of Technology* (Shandong Academy of Sciences). His major research interests are ultrahigh cycle fatigue and mechanical engineering.
E-mail: 260828436@qq.com

Ming, Zhang, born in 1987, is an associate professor of *Qilu University of Technology* (Shandong Academy of Sciences). He received his doctor degree from *Shandong University*. His main research direction is very high cycle fatigue.
Tel: 13853157623 E-mail: zm870623@foxmail.com

Meng-Li, Li, born in 1987. She received her doctor degree from *Shandong University.*
E-mail: miling001@163.com

Hai-Bao, Xie, born in 1997, He graduated from *Qilu University of Technology* (Shandong Academy of Sciences).
E-mail: 1351164877@qq.com

Li-Jun, Zhang, born in 1984, He received his bachelor degree from *Shandong University.* He worked in *Ningbo Geely Royal Engine Components Co.,Ltd*
E-mail: zhanglj@geely.com

Figures

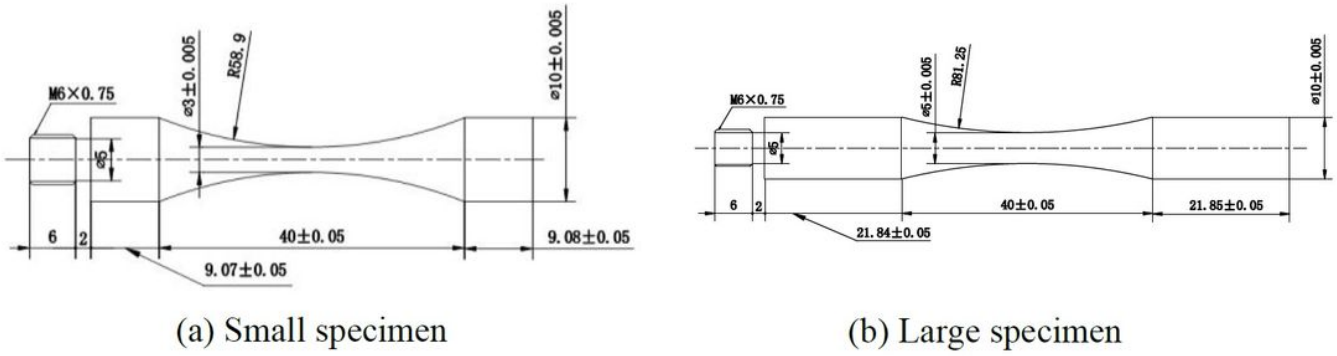

(a) Small specimen

(b) Large specimen

Figure 1

Specimen dimensions (in mm).

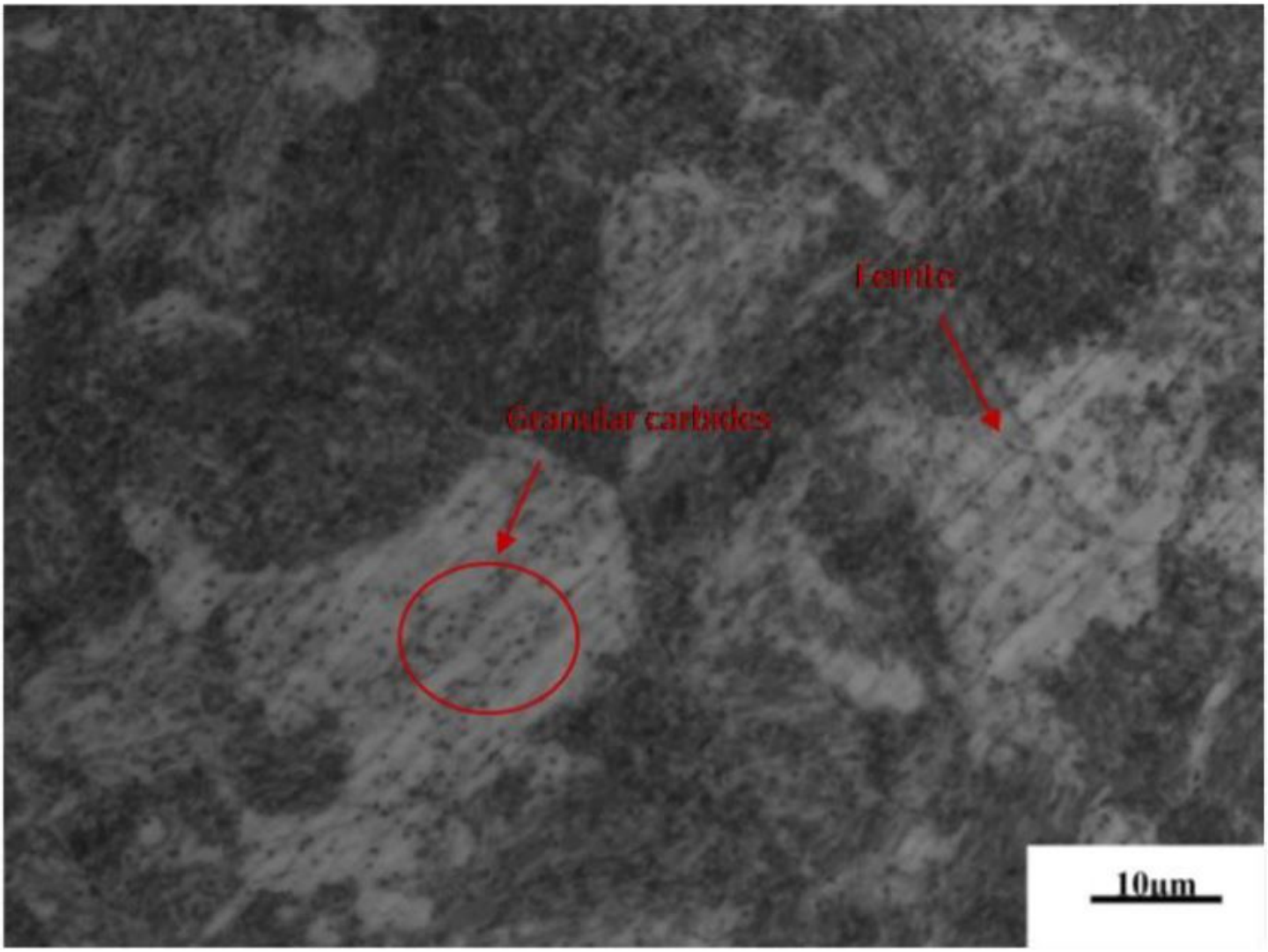

Figure 2

FV520B-I microstructure observation

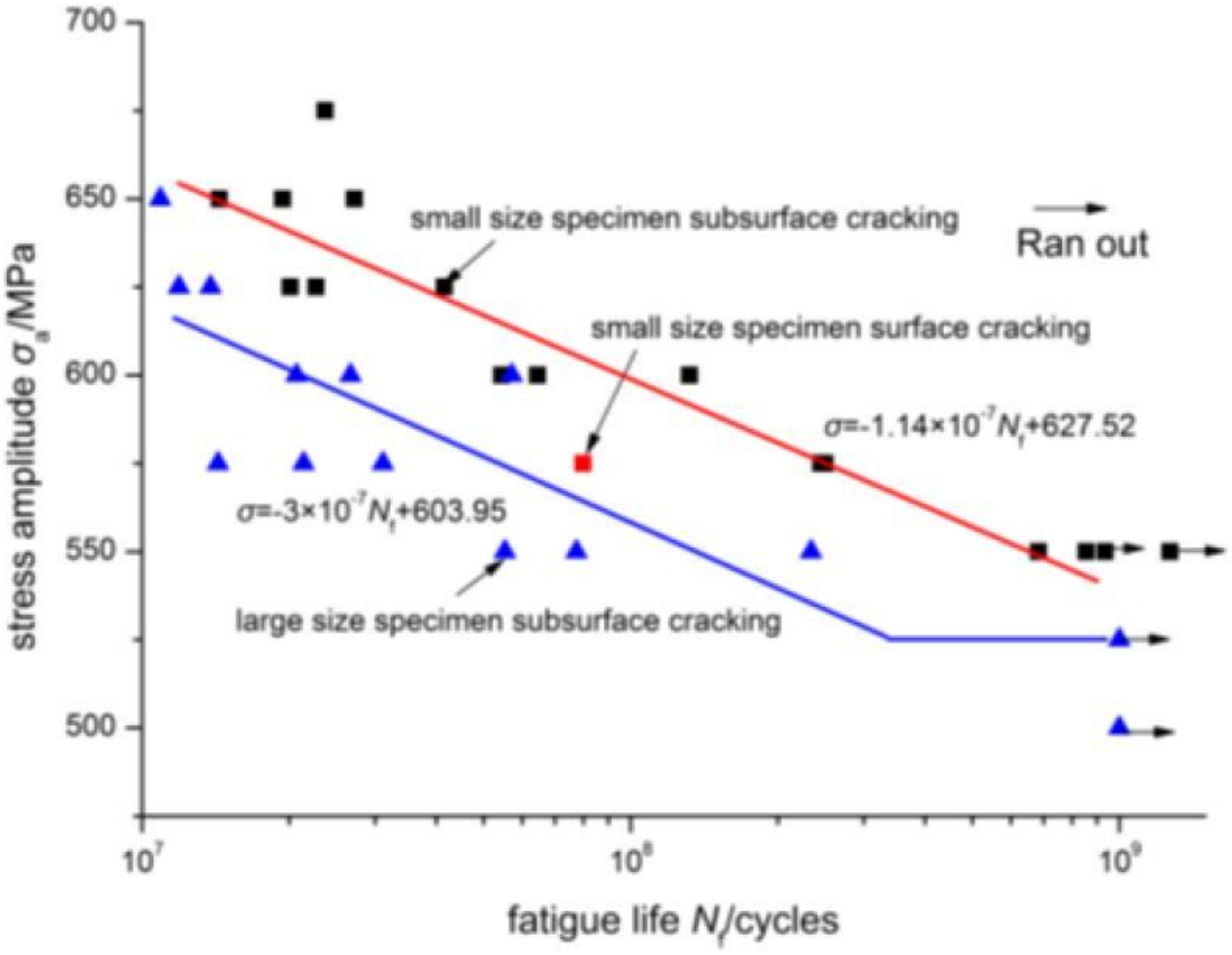

Figure 3

The VHCF S-N curves

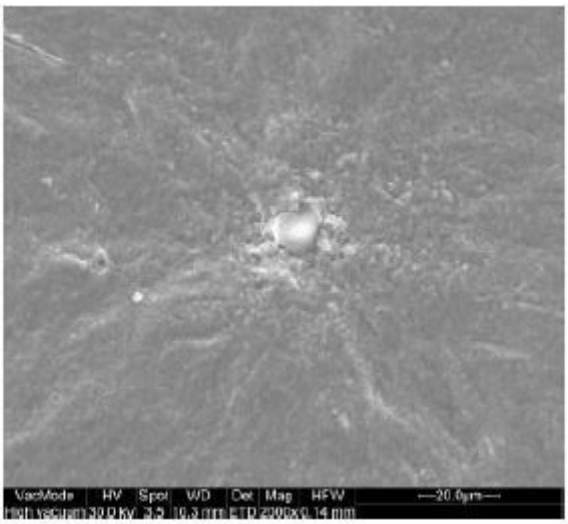

(a) Initiation from a single inclusion (σ_a=575MPa, N_f=1.43×10^7)

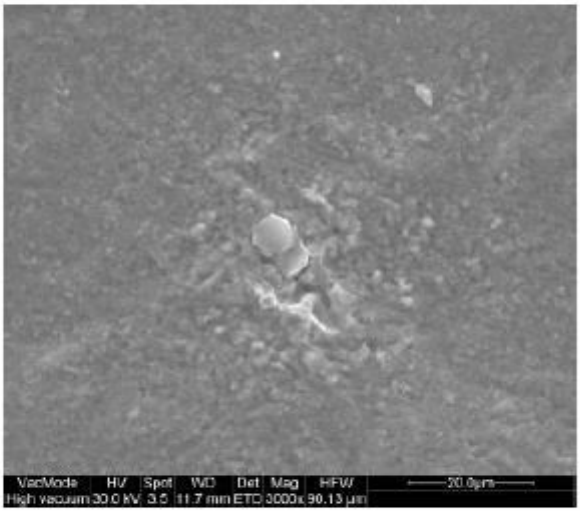

(b) Initiation from a cluster (σ_a=575MPa, N_f=2.14×10^7)

Figure 4

Initiation modes of FV520B-I VHCF cracks in large specimens

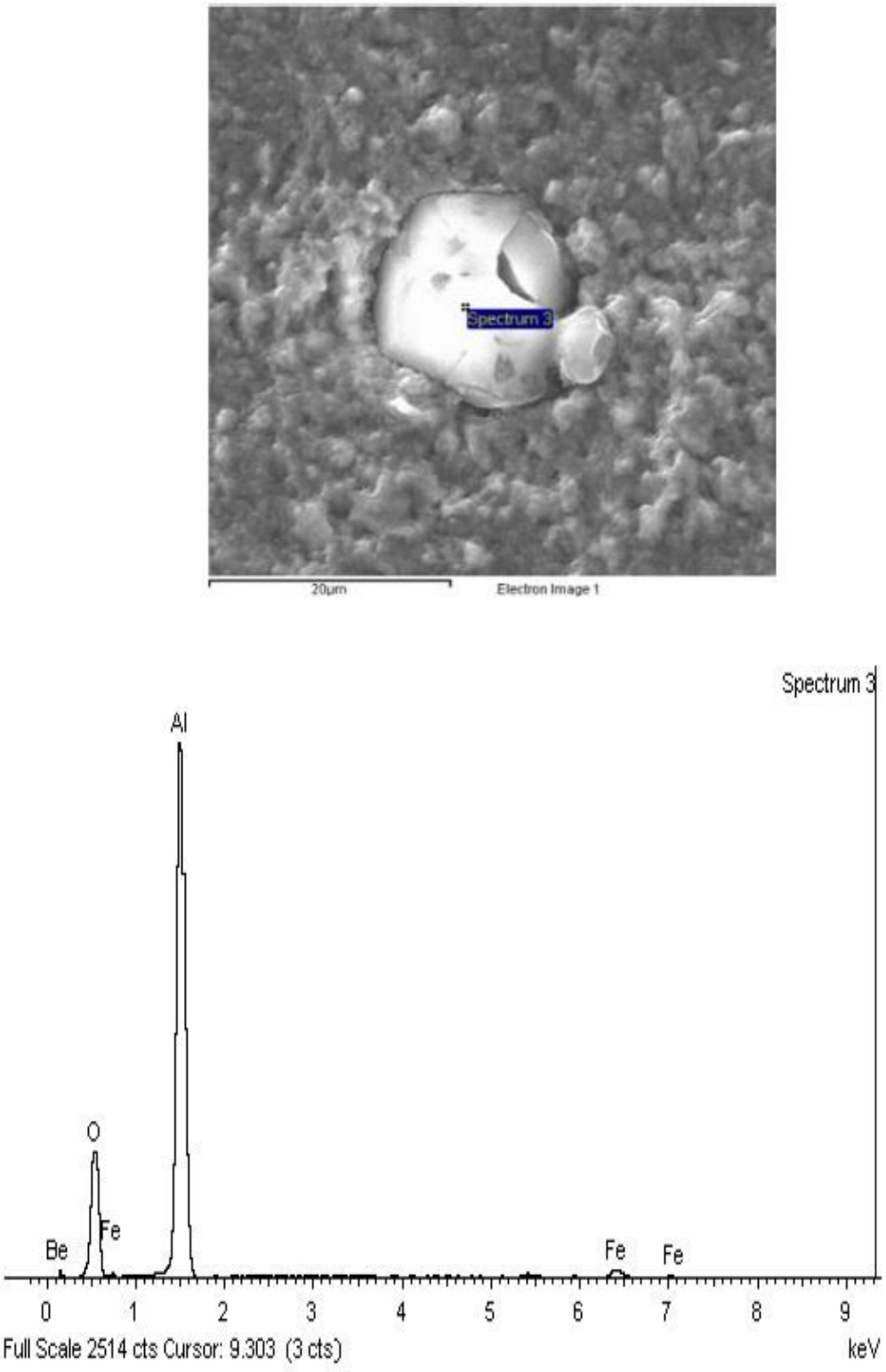

Figure 5

The energy spectrum analysis of an inclusion (σa=550MPa, Nf=5.53×107)

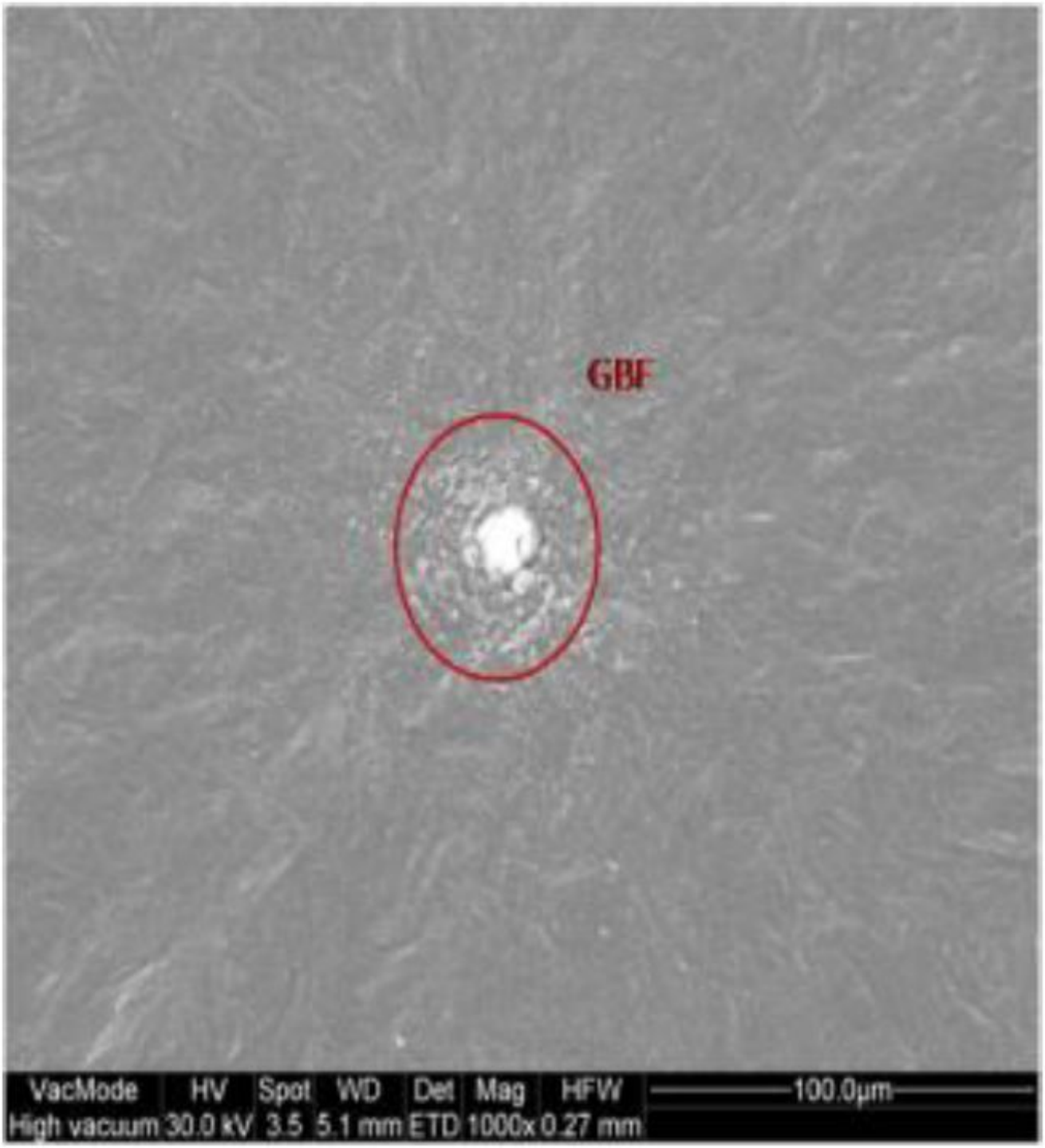

Figure 6

The GBF observation (σa=550MPa, Nf=5.53×107)

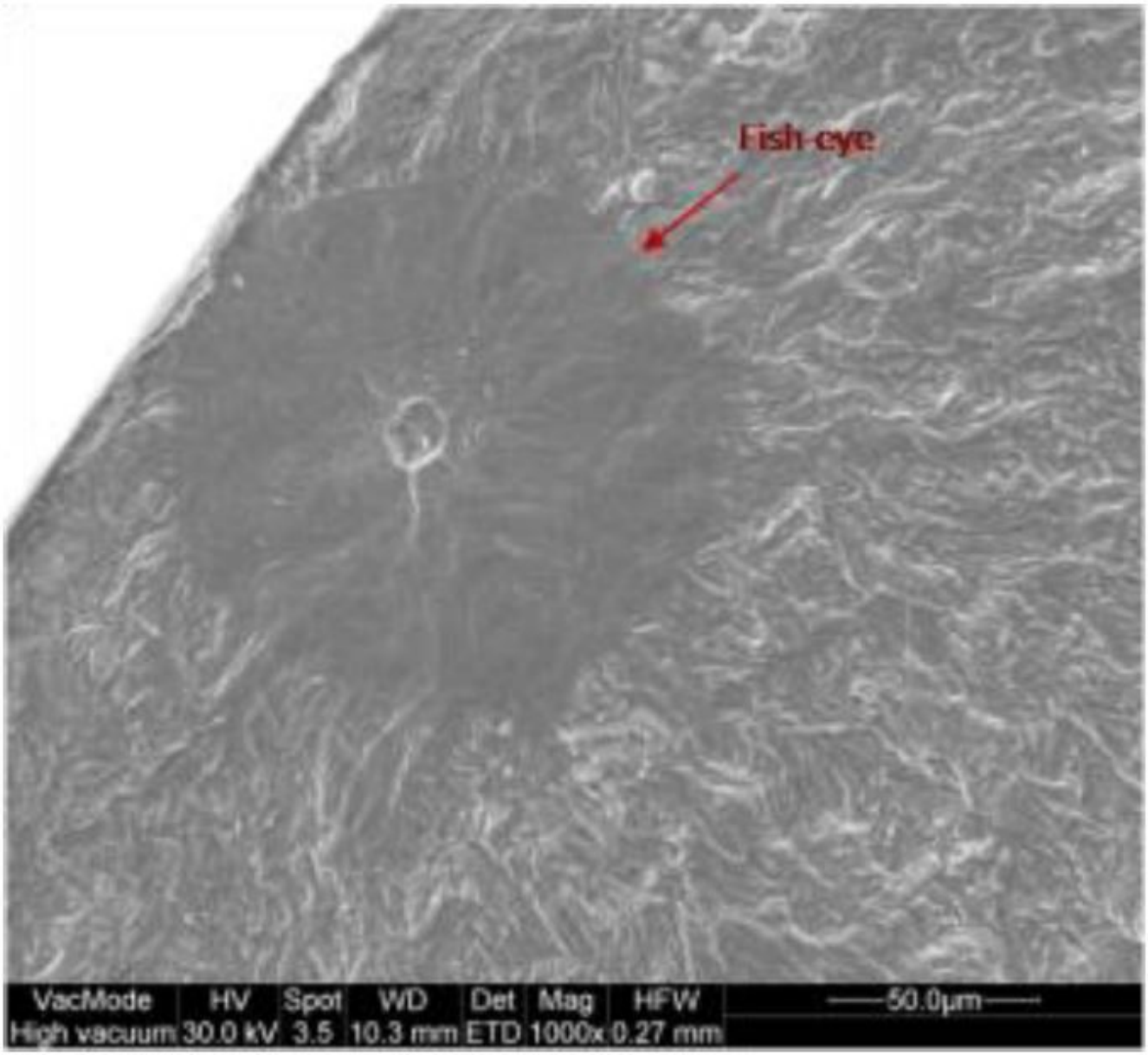

Figure 7

The fish-eye observation (σa=625MPa, Nf=1.19×107)

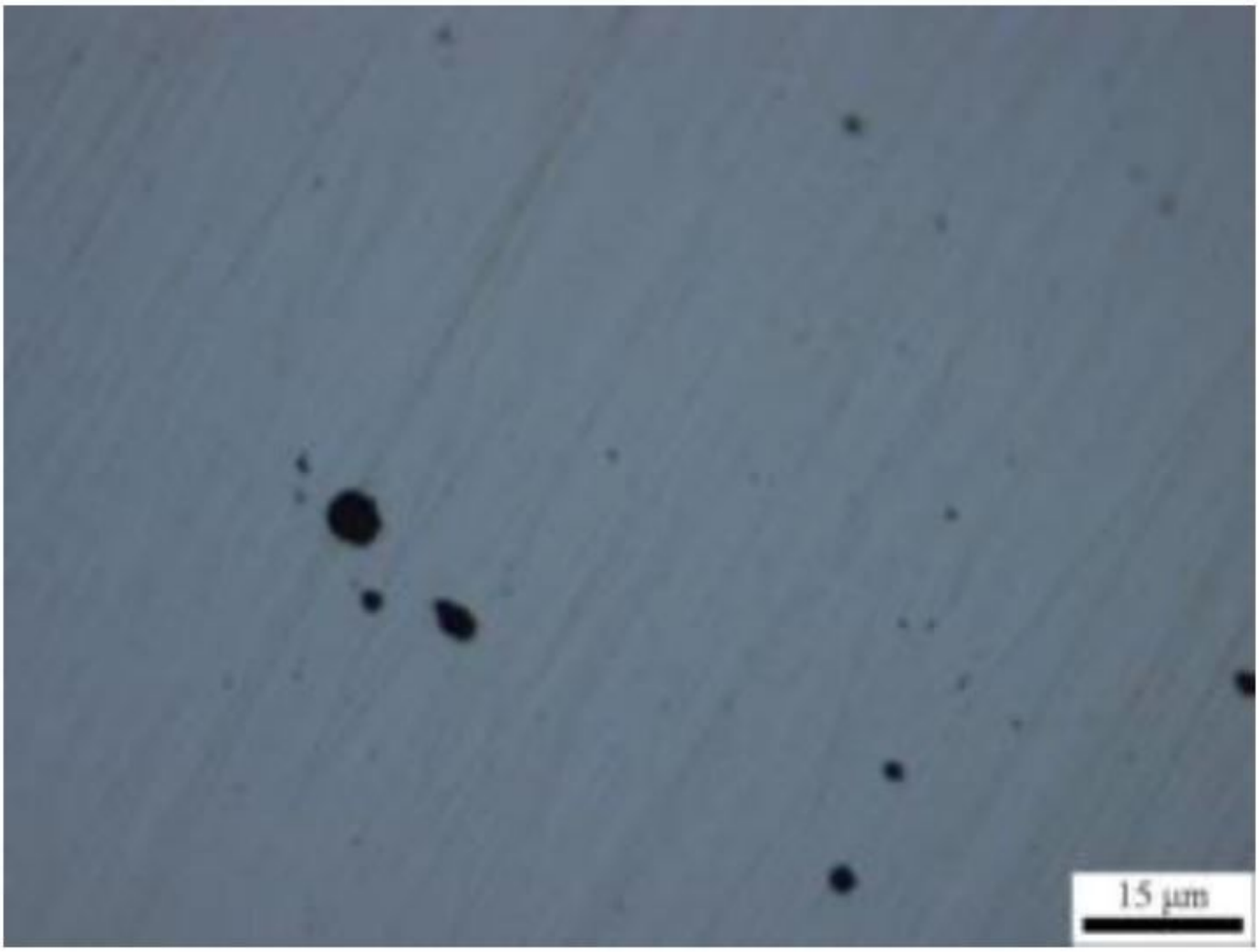

Figure 8

The inclusion situation of the 40th observation

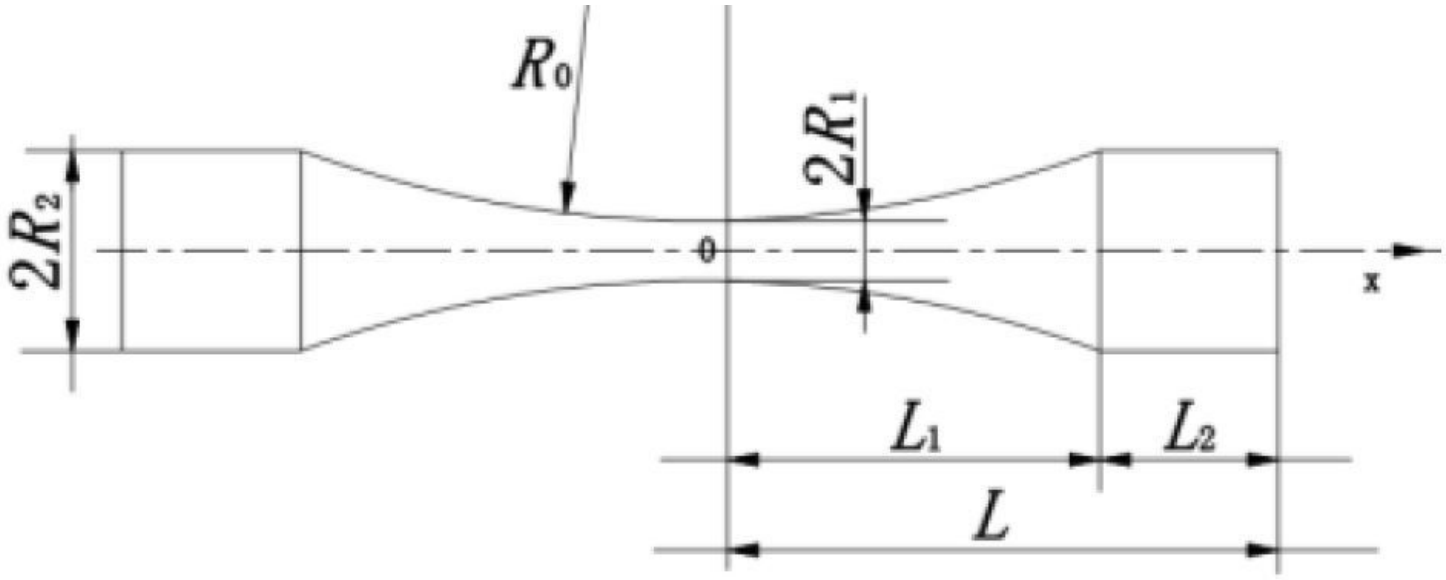

Figure 9

The shape of a funnel specimen

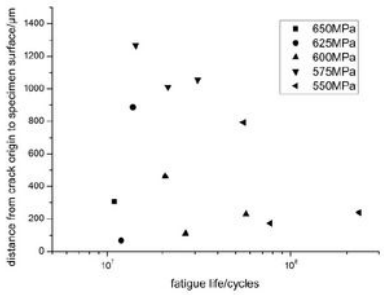

(a) Relationship with the distance from the crack origin to the specimen surface

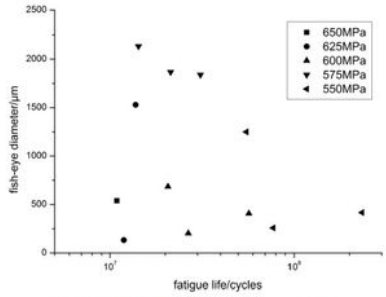

(b) Relationship with the fish-eye diameter

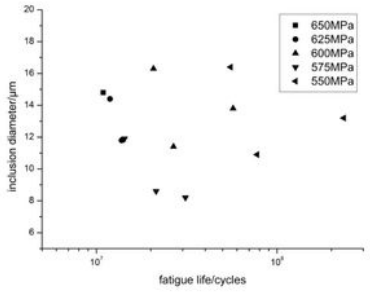

(c) Relationship with the inclusion diameter

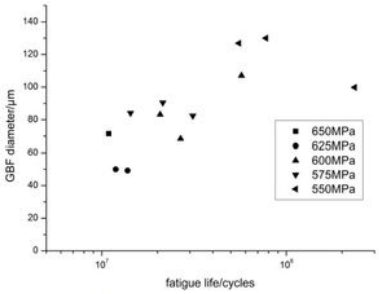

(d) Relationship with the GBF diameter

Figure 10

Relationships of VHCF life of large FV520B-I specimens with the characteristic area sizes

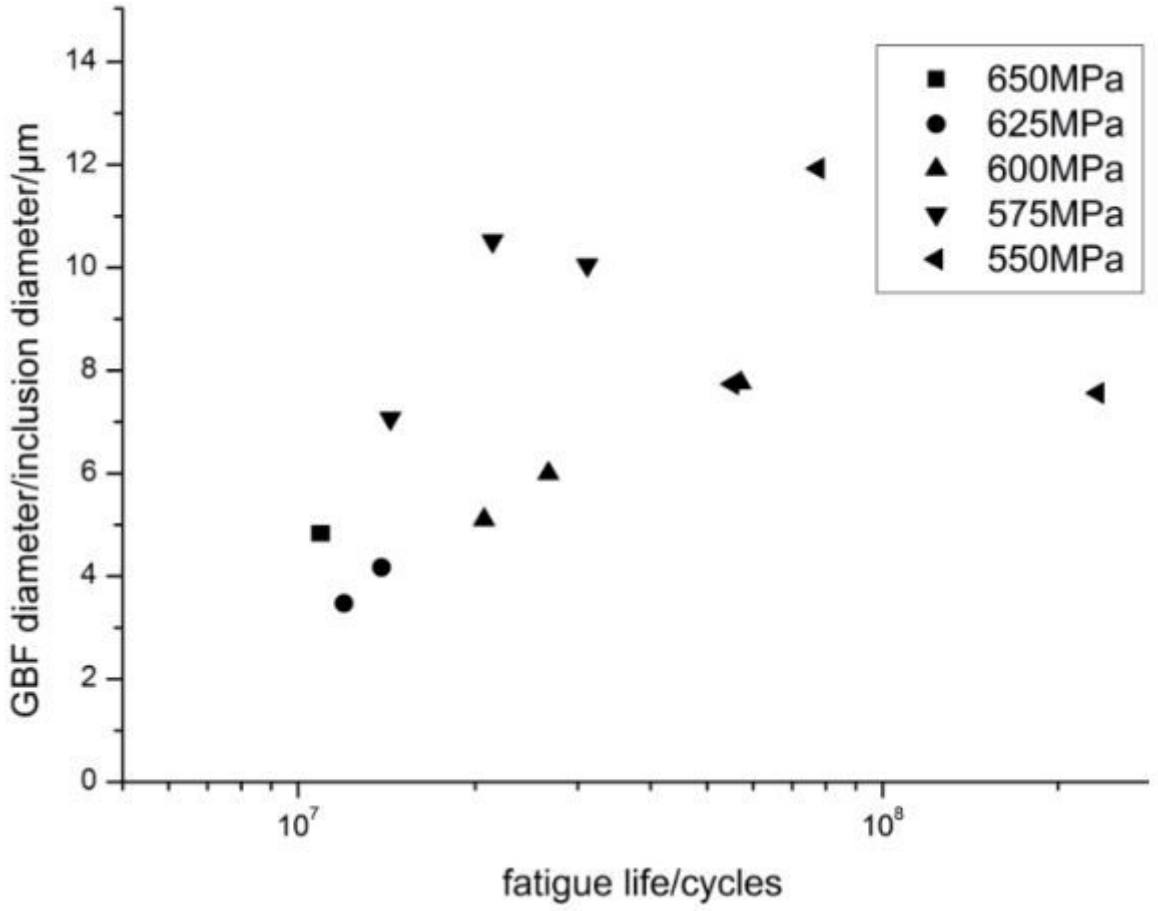

Figure 11

Relationships of VHCF life of large FV520B-I specimens with the ratio of the GBF diameter to the inclusion diameter

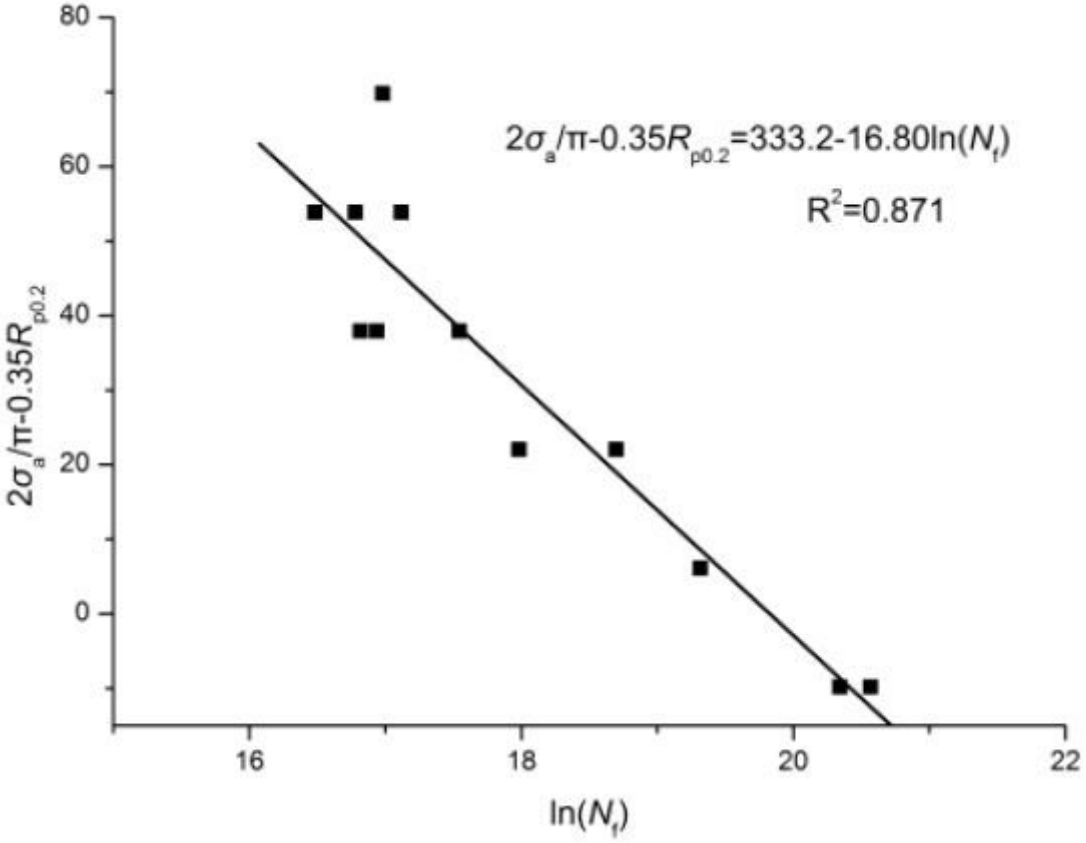

Figure 12

The fitting results of test data of small specimens by the corrosion fatigue crack initiation life model.

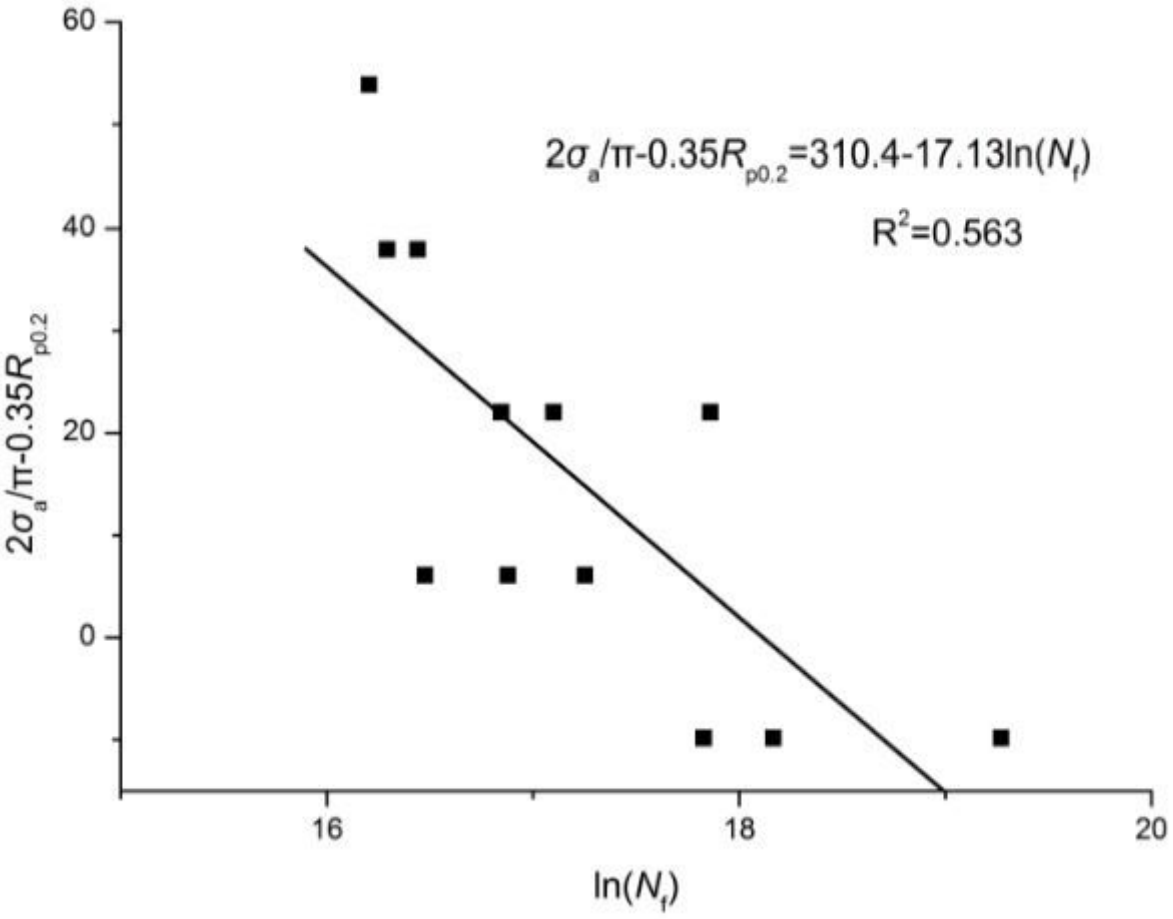

Figure 13

The fitting results of test data of large specimens by the CFC initiation life model